Wearable Mechatronic Ultrasound-Integrated AR Navigation System for Lumbar Puncture Guidance

Baichuan Jiang, *Member, IEEE*, Liam Wang, Keshuai Xu, *Graduate Student Member, IEEE*, Martin Hossbach, Alican Demir, Purnima Rajan, Russell H. Taylor, *Life Fellow, IEEE*, Abhay Moghekar, Pezhman Foroughi, Peter Kazanzides, *Member, IEEE*, and Emad M. Boctor, *Senior Member, IEEE*

***Abstract*—As one of the most commonly performed spinal interventions in routine clinical practice, lumbar punctures are usually done with only hand palpation and trial-and-error. Failures can prolong procedure time and introduce complications such as cerebrospinal fluid leaks and headaches. Therefore, an effective needle insertion guidance method is desired. In this work, we present a complete lumbar puncture guidance system with the integration of (1) a wearable mechatronic ultrasound imaging device, (2) volume-reconstruction and bone surface estimation algorithms and (3) two alternative augmented reality user interfaces for needle guidance, including a HoloLens-based and a tablet-based solution. We conducted a quantitative evaluation of the end-to-end navigation accuracy, which shows that our system can achieve an overall needle navigation accuracy of 2.83 mm and 2.76 mm for the Tablet-based and the HoloLens-based solutions, respectively. In addition, we conducted a preliminary user study to qualitatively evaluate the effectiveness and ergonomics of our system on lumbar phantoms. The results show that users were able to successfully reach the target in an average of 1.12 and 1.14 needle insertion attempts for Tablet-based and HoloLens-based systems, respectively, exhibiting the potential to reduce the failure rates of lumbar puncture procedures with the proposed lumbar-puncture guidance.**

***Index Terms*—Wearable devices, augmented reality, ultrasound imaging, image-guided procedure, spine intervention.**

I. Introduction

OVER 360,000 lumbar punctures (LP) are performed annually in emergency departments alone within the United States and the number is still increasing [1], [2]. During this procedure, the patient needs to bend forward to enlarge the inter-spinous gap, while the clinician tries to palpate the lumbar and locate the gap for needle insertion. It can be especially challenging for pregnant or obese patients who cannot sufficiently bend to open the inter-spinous gap, and for patients with severe spine malformations such as scoliosis. These difficulties can lead to prolonged treatment time and missing the initial needle placement. Repeated attempts may also increase the risk of iatrogenic complications [3]. According to [4], headache occurs in up to 40% of patients after lumbar puncture, and about 16% patients report issues with back pain. Other rarer ($< 1\%$) but more dangerous complications can also occur, including cranial neuropathies, nerve root injury, hematoma, CSF leak, meningitis, and prolonged backache and headaches (lasting up to 1 year) [3], [4], [5]. In addition, a traumatic LP procedure, with an estimated occurrence rate of 10%-30%, can result in CSF blood contamination which may introduce infection, confuse diagnostics and delay the proper treatment for the patient [6], [7].

To overcome these challenges, ultrasound guidance has been introduced for LP, which is shown to have a higher success rate (90.0%, with 2.07 needle passes on average), fewer traumatic LPs (10.7%), shorter procedural time (6.87 minutes) and is also radiation-free [8], [9], [10]. However, due to the complex shapes of the self-shadowing vertebrae and the static ultrasound scan from a single imaging pose, critical anatomical features such as inter-spinous gaps are often poorly visualized: (1) high acoustic attenuation from the bones will block out important anatomical features, (2) bone boundary features will not be completely shown in the images for the parts of the bone surface where the ultrasound beam incidence angle is large and (3) bone boundaries can be shown blurred with the early-and-late echo imaging artefacts due to elevational beam thickness and a large incidence angle. Therefore, the conventional ultrasound guidance approach can only provide minimum information for potential needle pathways. Additionally, since clinicians need to hold the ultrasound probe in one hand during the procedure, they cannot use both hands to stabilize the needle and control insertion depth [7].

Several approaches have been proposed to address these issues for ultrasound-guided spinal intervention. One of the most researched ideas is to register preoperative CT or MRI to the intraoperative ultrasound to provide complementary

Manuscript received 4 May 2023; revised 18 July 2023 and 21 August 2023; accepted 18 September 2023. Date of publication 27 September 2023; date of current version 27 October 2023. This article was recommended for publication by Associate Editor T. Haidegger and Editor P. Dario upon evaluation of the reviewers' comments. This work was supported in part by the National Science Foundation SCH:CAREER under Grant 1653322; in part by the National Institute of Health under Grant 1R43EB031731; and in part by Analog Devices Inc. Fellowship. *(Baichuan Jiang and Liam Wang contributed equally to this work.) (Corresponding authors: Peter Kazanzides; Emad M. Boctor.)*

This work involved human subjects or animals in its research. Approval of all ethical and experimental procedures and protocols was granted by the Johns Hopkins University, Homewood Institutional Review Board under Application No. HIRB00007467.

Baichuan Jiang, Liam Wang, Keshuai Xu, Russell H. Taylor, Peter Kazanzides, and Emad M. Boctor are with the Department of Computer Science, Johns Hopkins University, Baltimore, MD 21218 USA (e-mail: pkaz@jhu.edu; eboctor@jhu.edu).

Martin Hossbach, Alican Demir, Purnima Rajan, and Pezhman Foroughi are with Clear Guide Medical Inc., Baltimore, MD 21211 USA.

Abhay Moghekar is with the Department of Neurology, Johns Hopkins Medical Institute, Baltimore, MD 21205 USA.

Digital Object Identifier 10.1109/TMRB.2023.3319963

anatomical context information for needle insertion guidance [11], [12], [13]. However, the requirement for preoperative CT or MRI will increase the treatment time and cost. In [14], an atlas-based registration approach is taken to register the intra-operative ultrasound with a statistical shape model of lumbar vertebrae. While this approach may avoid the preoperative imaging requirement, it may not be suf ciently accurate when targeting patients with severe spine malformations or pediatric patients due to the limited modeling capability of the atlas. To completely remove the dependency on the preoperative scans while retaining the full anatomical context information, it is necessary to image the spine from multiple viewing angles and generate artifact-reduced ultrasound volumes. In the literature, this is proposed to be done freehand with external tracking devices or using an robot arm holding the probe [15], [16], [17], [18]. However, it is dif cult to maintain the image-anatomy relationship in the presence of patient motion and also may require the use of expensive, bulky robot arms. An alternative approach is to integrate an ultrasound element into the needle tip to provide guidance information from inside the needle and navigate through the anatomy [19], [20]. While this approach is registration-free and does not require bulky robot arms, it can only provide limited guidance information because the imaging feedback is acquired by rotational sweeping of the needle, which is often impractical when the needle is in deeper tissues or close to vital structures. Another approach utilizing augmented reality is presented in [21], where an ultrasound scan is used to create a virtual insertion plan to aid the user with spinal insertion, but this system only displays a holographic planning line that does not track with patient movement and does not contain anatomical context from ultrasound images. Similar AR-based approaches for needle-based spinal intervention have been presented but each has its limitations, such as utilizing preoperative CT which involves ionizing radiation [13], [22], or still relying on the user's hand operation for real-time image feedback during insertion [23].

To address the aforementioned issues, we present a new lumbar puncture needle guidance system that integrates our wearable mechatronic ultrasound device (an improved, tracking-friendly version from [24]) with two alternative augmented reality (AR)-based navigation interfaces (HoloLens-based and Tablet-based) and bone surface estimation algorithms [25] to provide accurate, real-time, and intuitive needle insertion planning and guidance for lumbar puncture. To the best of our knowledge, we are presenting the rst completely integrated LP-guidance system with wearable imaging hardware, image processing algorithm and UI components, that provides all of the following advantages:

- Hands-free automatic image acquisition.
- Does not require a pre-operative CT scan or use atlas-based registration of spine models.
- Does not require an expensive, bulky industrial robot arm.
- Provides multi-angle imaging of spine anatomy by controlling and measuring the exact geometry of ultrasound scanning motion.
- Maintains the accurate image-anatomy relationship in the presence of patient movement.
- Natural integration with image processing algorithms and AR user interfaces.

We rst introduce the individual system components and how each piece of hardware is integrated into a complete system with calibrations in Section II. Next, in Section III, we describe our quanti cation experiment for overall needle navigation accuracy and our user study on lumbar phantoms for qualitative evaluation of system usability. In Section IV, we provide discussions on experiment and user study results, followed by a summary of the research ndings and visions for future work in Section V.

II. Methodology

The overview of the full lumbar puncture guidance system is shown in Fig. 1. In this work, we have implemented two augmented reality interface variants for studying the effectiveness of different AR-guidance strategies. Within the LP-guidance system, a central communication laptop is connected to the image acquisition system and the navigation interfaces for data communication and control.

A. Wearable Ultrasound System Overview

In [24], we introduced a wearable ultrasound scanner designed for complex-shaped lumbar imaging which has a 2 degree-of-freedom (DOF) rotating and translating phased array transducer (Fig. 1(c)) that reduces shadows, increases the chance of US beams imaging with ideal incidence angles on bone surfaces and enlarges the eld-of-view for the lumbar anatomy. The wearable scanner is designed to be xed to the patient with bio-compatible adhesive and has a exible polymer acoustic standoff pad for the bottom part that conforms to the minor unevenness of the patient's skin. In this study, we used an improved version of the scanner with a similar mechanical design housing a custom 2.75 MHz phased array transducer, with an overall dimension of $110mm(L) \times 70mm(W) \times 48mm(H)$ and a weight of 307 grams. The ultrasound images were captured with an Ultrasonix SonixTablet.

To integrate the wearable scanner with the two navigation interfaces, three types of camera markers were attached to the scanner housing, including AprilTags [26] (19 mm × 19 mm), QR codes (25 mm × 25 mm), and infrared optical markers. The scanner housing is 3D printed with engraved markings so that AprilTags and QR codes can be accurately attached to known locations in the scanner coordinate frame. The AprilTags can be tracked by the Tablet camera, and the QR codes are used by the HoloLens 2.

B. Data Processing Pipeline

Immediately before the LP procedure, our wearable ultrasound imaging system collects a full scan of the patient's lumbar from varying insoni cation windows from the 2DOF device workspace. Then, the imaging data along with the positional encodings are transferred to the central communication laptop for image processing. The data will be processed and automatically sent to the Tablet-based or HoloLens-based navigation interfaces following

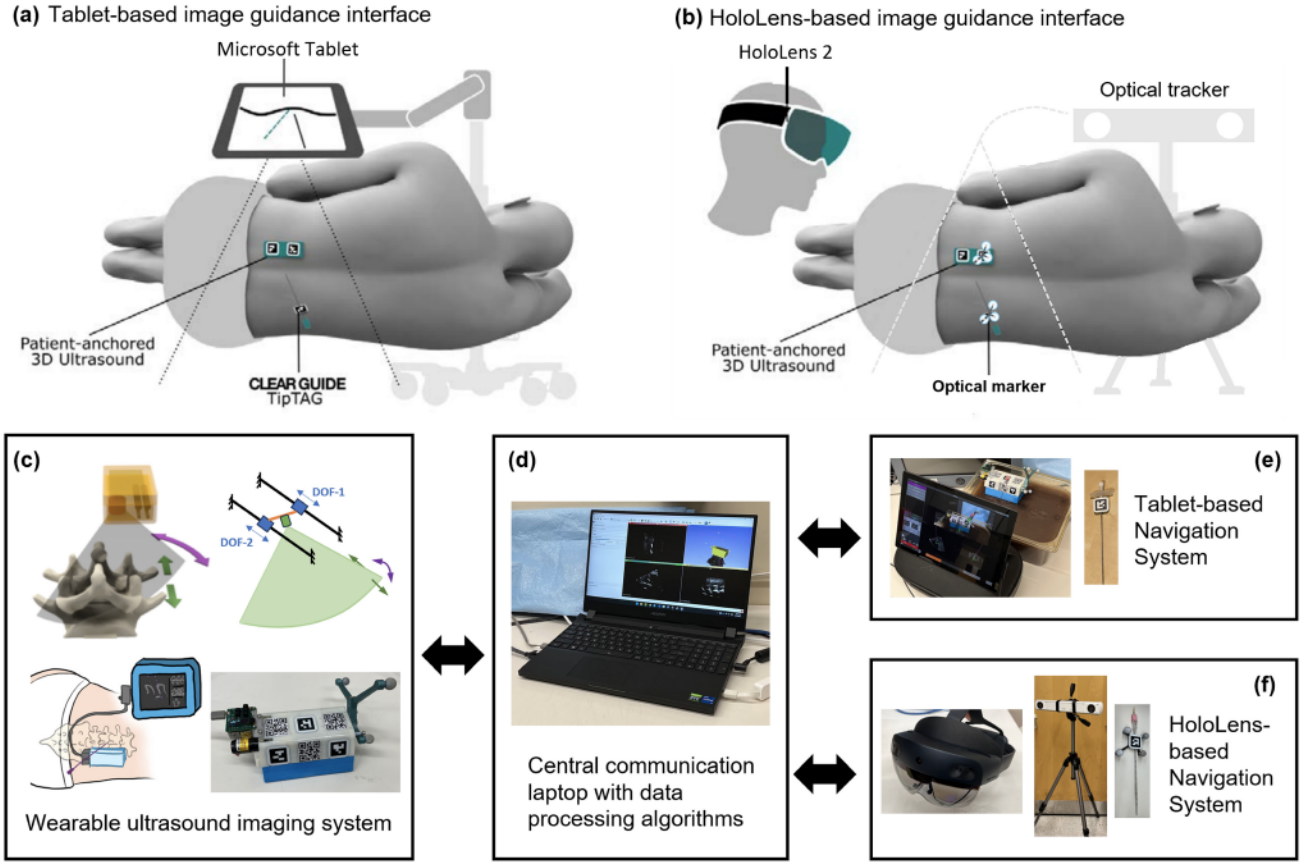

Fig. 1. Overview of the proposed lumbar puncture guidance system with two navigation interface variants: (a) Tablet-based solution, (b) HoloLens-based solution. The system components include (c) Wearable ultrasound image acquisition system, (d) data communication and processing workstation, and (e-f) two alternative navigation interfaces.

separate intermediate data processing pipelines as shown in Fig. 2.

Tablet-Interface Data Workflow: The Tablet-based navigation interface requires a reconstructed 3D ultrasound *volume* for needle path planning and guidance. During scanning, the spatial transformation for each 2D ultrasound image is recorded by the motor encoders and computed with scanner kinematics. Given the B-mode image data, corresponding spatial transformation, and pixel spacing information, we are able to reconstruct a 3D ultrasound volume following the algorithm described in [27] with the averaged voxel-nearest neighbor (VNN) method. Currently, our volumetric reconstruction algorithm takes about 90 seconds for the image processing of a whole scan, which is around 730 images with 9 angled linear sweeps, on a laptop computer with an Intel i7-12700k processor and RTX 3070 graphics card.

HoloLens-Interface Data Workflow: It is less intuitive to present the raw ultrasound data to the user in the HoloLens environment. Instead, we display a hologram of a 3D *mesh* representation of the spine surfaces generated from the ultrasound image data, as shown in Fig. 2(f). Here, we developed and integrated the surface estimation algorithm described in [25], where an aggregated feature extractor is applied on the raw 2D ultrasound image to generate a bone feature map (Fig. 2(b)), by taking advantage of the local phase information and the shadowing information within the image. Then, both the raw 2D US image and the feature map are fed into a spatio-temporal U-Net to produce a spine surface estimation heatmap. The network is trained using image data captured on a separate spine phantom to demonstrate algorithm generalization during the user study. We then reconstruct a bone surface estimation volume using the network output and the corresponding spatial transformation matrices. The reconstructed volume is further processed using automatic binary Otsu thresholding [28] followed by volumetric image closing and opening morphological operations. The binary 3D surface volume is then transformed into a mesh model via the Flying Edges algorithm [29] implemented within 3D Slicer [30] for needle path planning and guidance in the AR environment. Our bone surface estimation algorithm can create one complete 3D mesh in around 4 minutes including feature map generation, bone surface estimation and reconstruction. This is benchmarked on the same machine as the Tablet-method.

C. Tablet-Based Navigation Interface

Our tablet-based guidance strategy uses a Microsoft Surface Pro tablet system developed by Clear Guide Medical, as shown in Fig. 3. Three AprilTags are attached to the shell of the mechatronic US scanner and one AprilTag is attached to the needle to allow the rear-facing tablet camera to track the scanner and the needle in real-time.

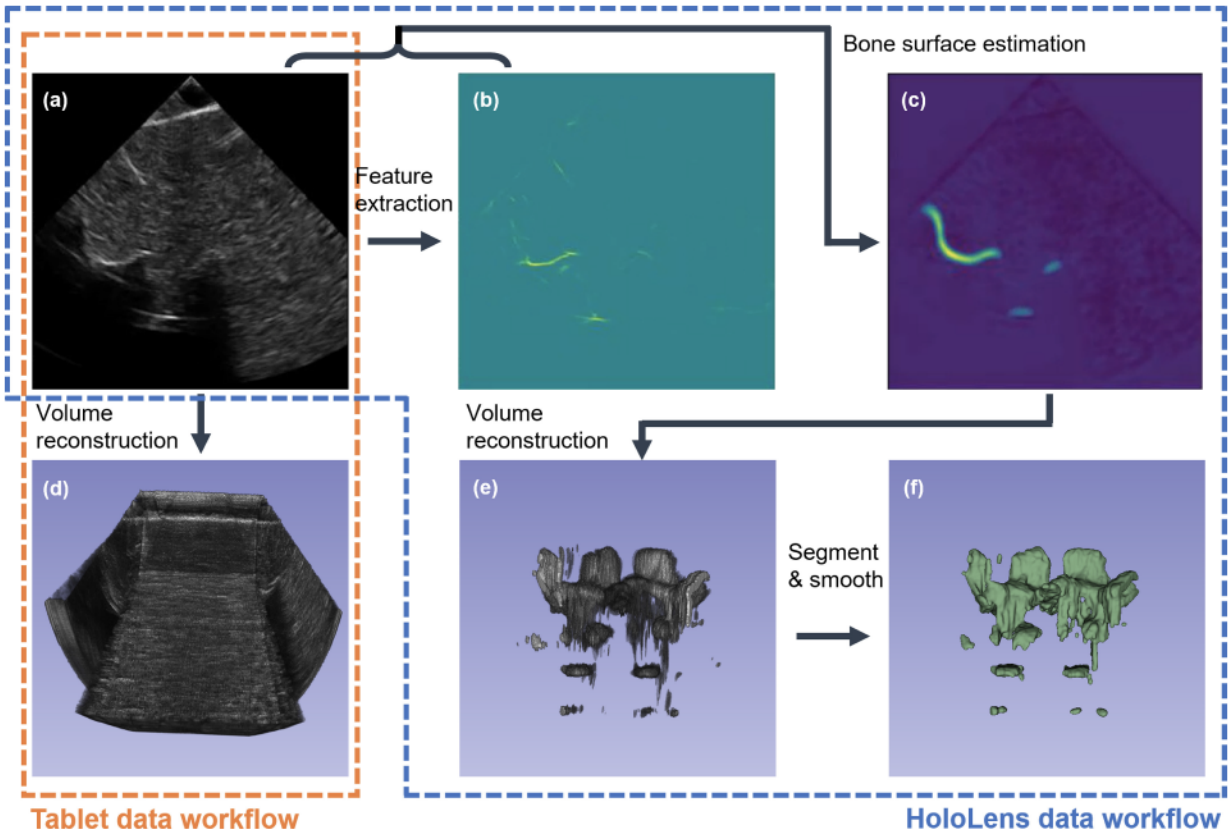

Fig. 2. Data processing workflows. *Tablet data workflow:* Raw images (a) are acquired by the wearable scanner along with transformation matrices, and ultrasound volume (d) can be reconstructed for needle planning. *HoloLens data workflow:* Raw images (a) are first used to extract feature image (b), and both images are used to compute a bone surface estimation map (c). The surface estimation maps can be reconstructed into a feature volume (e) and further processed as mesh surfaces (f) for the HoloLens application.

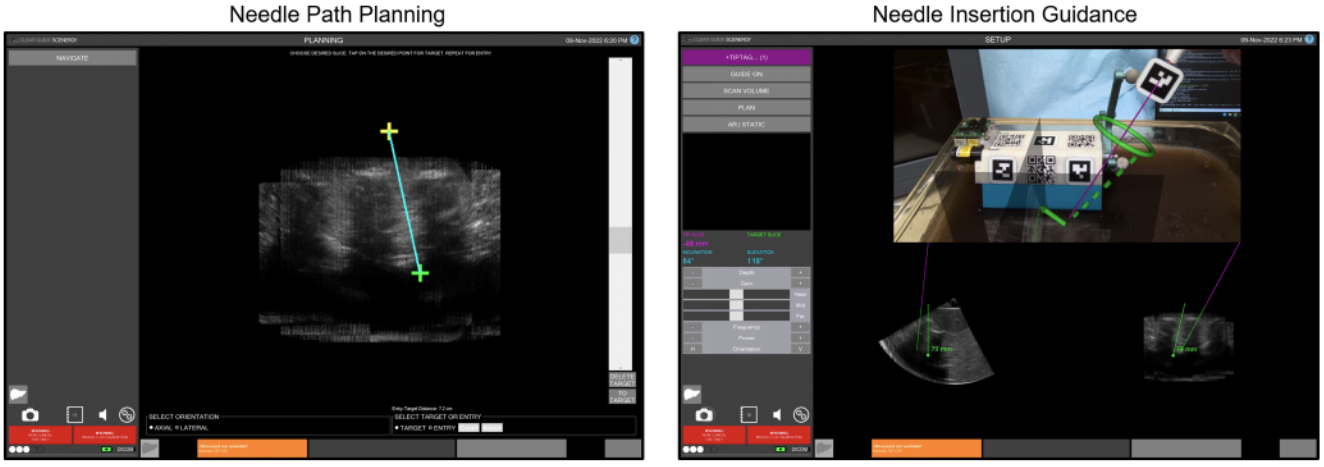

Fig. 3. Tablet-based navigation interface overview. *Left*: Using the path planning interface, an entry point (yellow) and a target point (green) can be selected. *Right*: During needle insertion, a solid green arrow is drawn from the tracked needle tip to the planned entry point. The green dotted line indicates the target needle angle, and the green torus represents the angular alignment error in the camera depth direction.

Path Planning Interface: For the tablet guidance system, an ultrasound scan is performed and the scan volume is reconstructed. This 3D US volume is sent from the central communication laptop to the tablet over Wi-Fi. Using the touchscreen planning interface on the tablet (Fig. 3 *Left*), the clinician can scroll through slices of the 3D ultrasound volume in either axial or sagittal view and select an entry point and a target point within the volume, and thereby position a "virtual" guidance line at a specific pose in 3D space that serves as a navigation guide line for the actual LP needle placement.

Insertion Guidance Interface: As shown in Fig. 3 (*Right*), the top half of the tablet screen displays the rear camera feed with augmented reality overlays of in-place orthogonal ultrasound slices. At the bottom of the screen, two orthogonal static 2D US slices are displayed with an overlaid green line representing the planned needle trajectory. The images are the axial

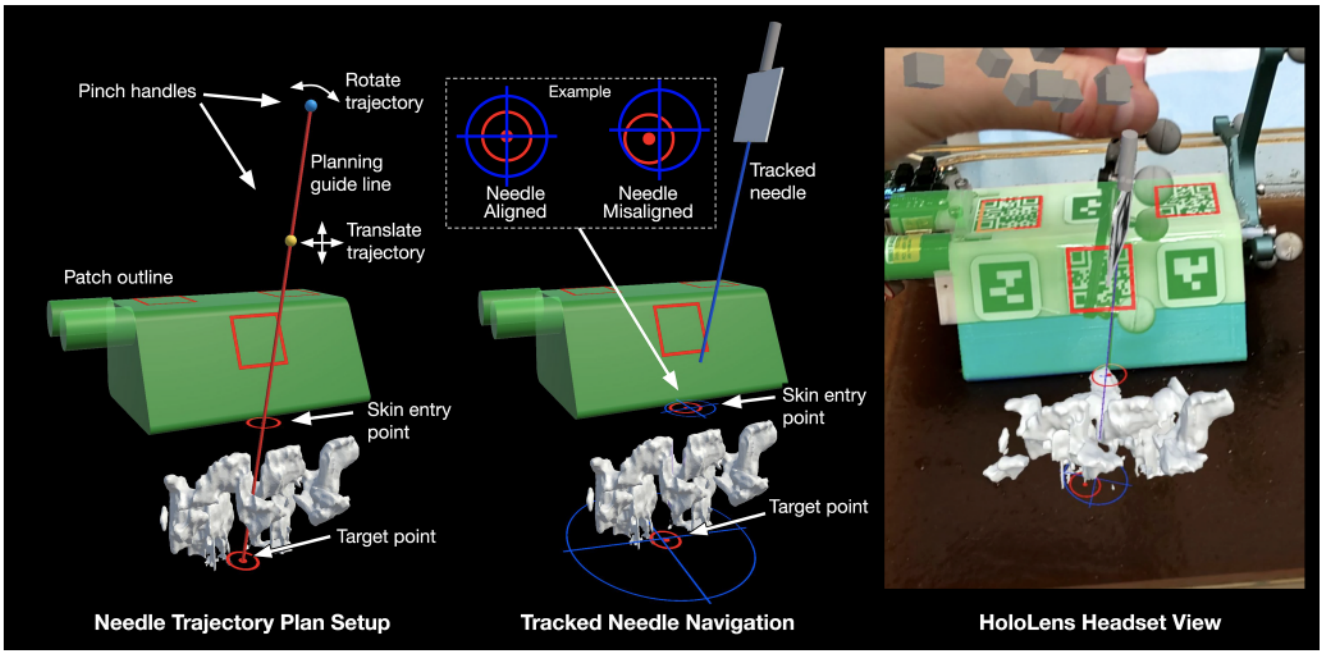

Fig. 4. HoloLens-based navigation interface overview. *Left:* In planning mode, the user selects a planned needle trajectory by positioning the red planning guide line. The HoloLens 2 built-in hand tracking allows the user to pinch and drag the yellow and teal grab handles. The yellow sphere translates the line, while the teal sphere rotates the line around the target point. *Center:* During needle insertion, the user can follow a trajectory plan by lining up the blue crosshairs (expected path of the tracked needle) with the red circular visual cues (trajectory plan path). *Right:* The scanner outline (green) and tracked needle position are displayed as holograms to allow the user to verify tracking accuracy, with the same spine model shown in *Left*.

and sagittal views of the reconstructed volume and are selected such that they contain the target point. During the procedure, the tracked needle position is simultaneously shown as purple lines in all three sections of the tablet display. In the top augmented reality screen section, a green arrow is drawn from the tracked needle tip to the planned entry point on the skin surface, allowing the clinician to position the needle tip in the correct starting location. A dotted line showing the angle of the planned trajectory allows the clinician to pivot the needle to obtain correct left/right alignment. Angle alignment error in the forward/backward direction is visualized via a green torus encircling the tracked needle that shrinks as alignment improves. After the needle is in proper alignment with its tip on the skin surface, the needle insertion progress can be monitored on the lower screen in the two orthogonal US slice views, where the planned trajectory and the tracked needle's expected path are overlaid as green lines. The distance to the target location is also shown in real-time.

D. HoloLens-Based Navigation Interface

Our head-mounted display (HMD) guidance strategy uses a wireless Microsoft HoloLens 2 system running a custom application developed using the Unity 3D game engine, which is now open-sourced.[1]

The front-facing cameras on the HoloLens 2 track the location of the wearable scanner using three QR codes, as in Fig. 1(c). A fusionTrack 500 (Atracsys LLC, Puidoux, Switzerland) optical tracking system is used to track the position of the LP needle relative to the scanner in real-time using the optical marker attached to both the needle and the scanner.

The ultrasound image data is first processed as shown in Fig. 2, and the 3D mesh is sent from the central communication laptop to the HoloLens over Wi-Fi. The mesh is projected as a hologram at the corresponding location of the actual vertebrae under the patient's skin. This interface offers the user an intuitive "X-Ray" view of the lumbar vertebrae and the inter-spinous gap.

Next, the clinician sets up a planned needle trajectory through the inter-spinous gap by positioning a virtual "planning guide line" using intuitive pinch-and-drag gestures (Fig. 4 *Left*). This virtual planning guide line can be positioned and angled using the pinch handles. The hand tracking input is smoothed to allow for precise positioning of the target trajectory even if the user's hand is unsteady.

To perform the needle insertion, the "planning guide line" is first turned off, and then the tracked LP needle is brought into the view of the fusionTrack 500 optical tracking system. The HoloLens displays a virtual overlay on top of the tracked needle in real-time. Virtual visual cues allow the clinician to correct needle alignment error during insertion (Fig. 4 *Center* and *Right*). Two sets of crosshairs and red circles are displayed: one at the surface of the patient's skin, and the other at the target depth of the trajectory plan. This ensures that both the insertion angle and the target point of the planned trajectory can be reached. The blue crosshairs represent the expected path of the tracked needle. The red circles represent the planned skin entry point and target point location. The clinician's task is to align the blue tracked needle crosshairs with the red circles and advance to the target position. As the

[1] https://github.com/liamjwang/lp-mr

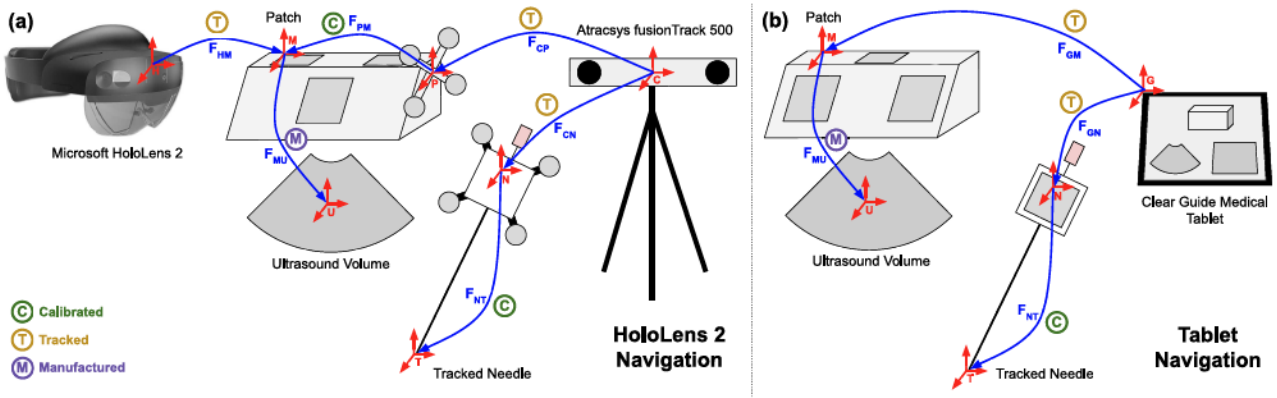

Fig. 5. Transformation chain diagram for (a) HoloLens 2 navigation system and (b) Tablet-based navigation system. Transforms marked with green "C" are identi ed with calibration experiments introduced in Section II-E, while the rest of the transforms are obtained either through tracking device speci cations (marked with yellow "T") or hardware manufacturing data (marked with purple "M").

tracked needle is inserted and approaches the target, the blue crosshairs shrink, allowing the user to accurately visualize the distance to the target.

E. System Integration and Calibration

To seamlessly integrate different pieces of hardware into a uni ed system, key transformations that link each component need to be computed, which are summarized in Fig. 5. Based on the nature of each transformation, we can group these transformations into three categories: (1) identi ed via calibration experiments, (2) known from tracking hardware, or (3) identi ed via manufactured geometry and further calibration.

For relevant transforms, calibration is conducted as follows:

1) The translational part of the transformation from needle marker (either AprilTag or QR code) to needle tip F_{NT} were calibrated via a standard pivot-type calibration on the needle tip. The orientation of the needle is calibrated by performing an additional pivot calibration on a blunt pointer attached on the other end of the needle, as shown in Fig. 1(f), which is used to compute the needle axis orientation in the marker's coordinate frame.
2) The transformation from the wearable scanner device to the externally attached optical marker F_{PM} was calibrated by using a calibrated rigid pointer (mathematically equivalent to the clinical needle), to touch a set of points on the locations p_M w.r.t. the local coordinate M (Fig. 5(a)) on the scanner housing, such that p_M is known from the CAD model of the device. Let us denote p_{tip} as the needle tip location in the local coordinates of the needle tip, i.e., $p_{tip} = [\mathbf{0}, 1]$; we can then establish the following equation:

$$F_{PM} \cdot p_M = F_{CP}^{-1} \cdot F_{CN} \cdot F_{NT} \cdot p_{tip} \tag{1}$$

where the only unknown is F_{PM}, so we can take the transformations F_{CP} and F_{CN} known from the optical tracker to perform point cloud registration to solve for F_{PM}.

3) The transformation between the ultrasound volume and the scanner coordinates F_{MU} was calculated using the known manufactured geometry of the mechanical components within the scanner device combined with an extra calibration step to identify an empirical offset value for the ultrasound transducer imaging origin. The origin was identi ed via an object scanning experiment which took place in a Cone-Beam CT (CBCT) environment. During the experiment, we manually adjusted this offset value to align the reconstructed ultrasound volume to the ground truth location of the object with respect to scanner coordinate identi ed in CBCT.

III. Experiments and Results

A. System Navigation Accuracy Assessment

To quantitatively evaluate the overall navigation accuracy of the imaging system with our AR interfaces, we performed two-stage evaluation: we rst identi ed the needle tracking accuracy by itself, then we performed an end-to-end navigation accuracy assessment using the method shown in Fig. 6.

Tracking Accuracy Assessment Workflow: As the rst stage of evaluation, we assess the needle tracking accuracy achieved by either the monocular rear-facing camera of the tablet or the stereo camera of the Atracsys optical tracker. After an LP needle was calibrated as described in Section II-E using either of the tracking systems, we moved the tip to a new location and performed a pivoting motion while recording the poses of the AprilTag or optical marker attached to the needle. A point cloud of the needle tip estimations was generated and its standard deviation is considered as the needle tracking accuracy achieved by the corresponding tracker (tablet rear-facing camera or optical stereo camera).

End-to-End Navigation Accuracy Assessment Workflow: For the second stage of evaluation, we used a 3D printed multi-cross-wire phantom as shown in Fig. 6(c), which is placed in a water- lled tank. The wearable scanner is placed on the phantom and scans the cross-wire features. The crossing "wires" have 2 mm diameter and indentations at the cross-wire

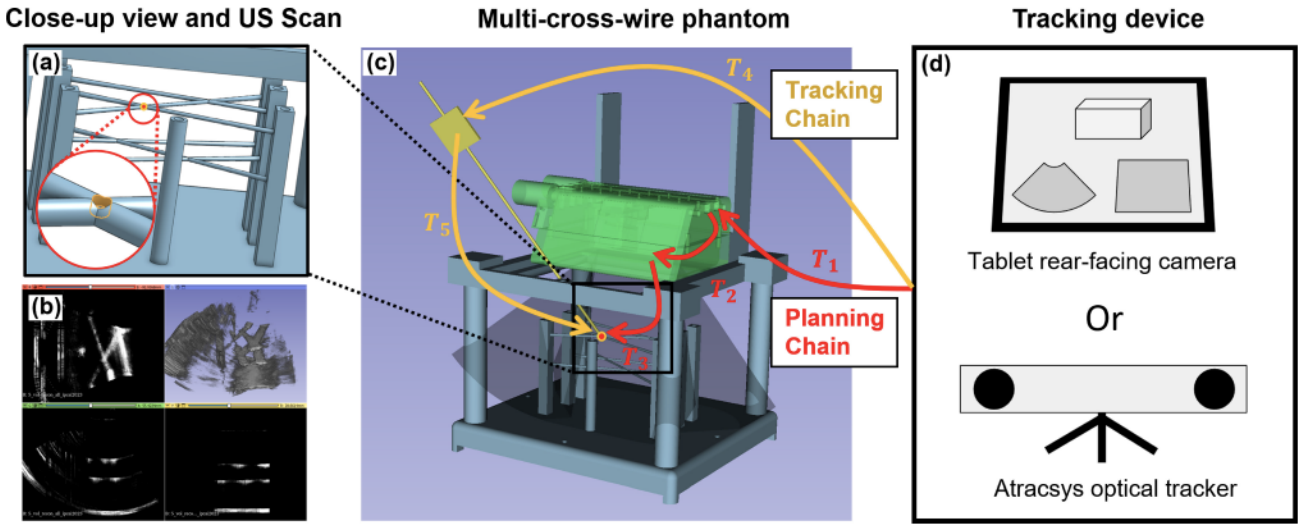

Fig. 6. System navigation accuracy quantification experiment setup. (a) A multi-cross-wire phantom was 3D printed with indentations at the cross-wire points for securely placing the needle tip at the accurate location. (b) Volumetric ultrasound scan using the wearable scanner. (c-d) Overall experiment setup: the transformation chain from both tracking the needle and planning in the ultrasound volume should ideally reach the same point, as the needle is precisely placed in the wire-crossing point when taking measurements. $T1$: F_{GM} or F_{CP}; $T2$: F_{MU} or $F_{PM} \cdot F_{MU}$; $T3$: Cross-point location in ultrasound volume annotated by user; $T4$: F_{GM} or F_{CN}; $T5$: F_{NT}.

intersections as in Fig. 6(a), so that the needle tip can be repeatably and precisely placed at the intersection points.

Next, to evaluate the overall accuracy of the navigation, we scanned the multi-cross-wire phantom and reconstructed the ultrasound volume as in Fig. 6(b). Then we placed the needle tip onto the indentation at each cross-wire point and took a snapshot of the current tracking transformations. For a system without error, the needle tip location computed by the tracking transformations w.r.t. the scanner base coordinates should be at the same cross-wire points in the ultrasound volume w.r.t the scanner base coordinates, i.e., the tracking chain and planning chain should reach the same point as described in Fig. 6(c-d).

Let us denote p_{US} as the cross-wire point location in the Ultrasound volume local coordinate "U". The system overall navigation error for the tablet solution, ϵ_{tablet}, can be computed by:

$$\epsilon_{tablet} = \left| F_{MU} \cdot p_{US} - F_{GM}^{-1} \cdot F_{GN} \cdot F_{NT} \cdot p_{tip} \right| \quad (2)$$

whereas the overall navigation error for the HoloLens solution, $\epsilon_{hololens}$, can be similarly computed by:

$$\epsilon_{hololens} = \left| F_{MU} \cdot p_{US} - F_{PM}^{-1} \cdot F_{CP}^{-1} \cdot F_{CN} \cdot F_{NT} \cdot p_{tip} \right| \quad (3)$$

following the transformation definitions introduced in Fig. 5.

To identify the cross-wire point location p_{US} in the ultrasound volume, we used a back-and-forth scrolling technique, picking multiple points along the wires and fitting lines to determine the cross-wire intersection points. To reduce human error in selecting the cross-wire point in the ultrasound image, we also repeated this action with each cross-wire point 5 times. Then, to evaluate the accuracy at different needle tracking poses and different locations within the ultrasound field of view, we repeated the above procedure 3 times with varying needle poses at each of the 4 cross-wire points. For each of the needle pose, we can compute the current system error following equations (2) or (3) and report its average and standard deviation as the overall needle-tip placement accuracy.

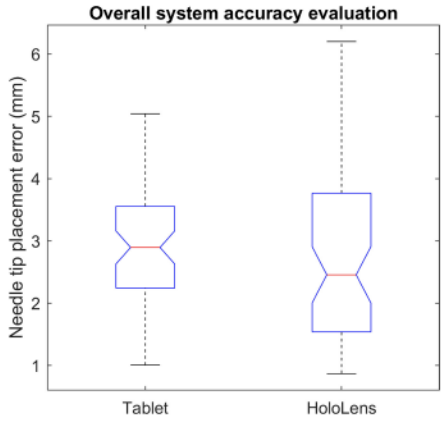

Fig. 7. Result for overall system navigation accuracy assessment. The maximum navigation errors in this experiment are 5.04 mm and 6.20 mm for Tablet and HoloLens solutions, respectively.

System Accuracy Assessments Results: For the first stage evaluation, the standard deviation for needle tip estimation during the pivoting motion was 0.46 mm for tablet camera-based tracking and 0.13 mm for optical tracker-based tracking, with a transformation sample size of 1000. For the second stage end-to-end accuracy evaluation, the average system accuracy for the tablet-based solution is 2.83 mm with a standard deviation of 0.86 mm, and for the HoloLens-based solution (using Atracsys optical tracker), it is 2.77 mm with a standard deviation of 1.43 mm. A box-plot result is shown in Fig. 7. This result represents the accumulated navigation error of reaching a known point in space guided by our wearable ultrasound navigation systems.

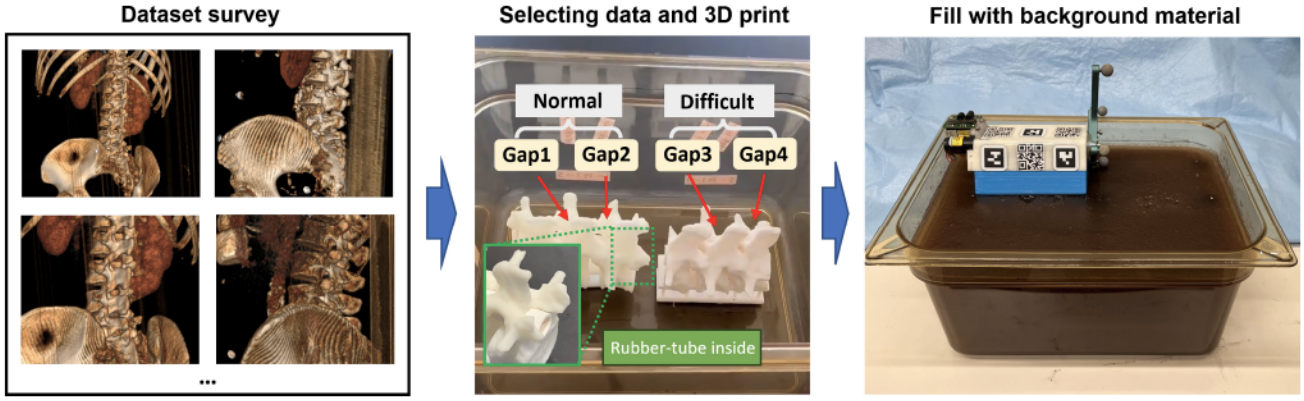

Fig. 8. User study phantom setup. A spine anatomy survey is conducted on a CT dataset (*Left*), and both a normal and a difficult case were chosen to be 3D printed with rubber tubes filling vertebral foramen (*Middle*). In the end, background material was filled to mimic the human soft tissue (*Right*).

B. User Study Design for System Usability Assessment

In addition to assessing the system's overall image guidance accuracy, we also conducted a user study to qualitatively evaluate the effectiveness of our navigation system in performing lumbar puncture procedures, and to study the user experience when using our two AR-based navigation interfaces.

Phantom Preparation: A user study phantom was created following the workflow shown in Fig. 8. First, we completed an anatomical survey of a public abdominal CT dataset [31], [32] and identified one subject with an average-size inter-spinous gap for lumbar puncture ("Normal" case, hole diameter ∼13 mm) and the other subject with a smaller inter-spinous gap ("Difficult" case, hole diameter ∼9 mm). Three lumbar vertebrae (L2-L4) were segmented from the up-sampled high-resolution CT images and 3D printed with Formlabs Rigid 4000 v1 material. A rubber tube (15 mm outer diameter, 1.75 mm thickness) was inserted into the vertebral foramen to simulate the feeling of inserting through the supra-spinous ligament when reaching the subarachnoid space, which allows an easy identification of a successful needle insertion. The lumbar models were glued to the bottom of the container and filled with gelatin-based soft-tissue-mimicking material. The phantom material was made according to the recipe described in [33] and an example ultrasound image of our custom-made phantom is shown in Fig. 2(a). We have open-sourced the segmented lumbar models used in our study to allow other researchers to evaluate with the same anatomy.[2]

Study Design: For our user study, we recruited a total of 22 participants, the majority of whom had limited or no prior experience with AR/VR applications or ultrasound imaging. The ultrasound data were acquired and processed following the data processing pipeline shown in Fig. 2 before each experiment to expedite the user trials. The order of the two navigation interfaces to be tested was randomly chosen for each user to eliminate learning effects (i.e., users getting more experienced with LPs during later trials).

For each user trial, a study team member first introduced the project background and tasks. Next, for the first navigation interface, a study team member demonstrated how to use the system. Then, to evaluate the usability of the planning interface, the user attempted to make a needle insertion plan. To separately evaluate the planning and navigation aspects of each interface, "expert" plans were provided by the study team member and were used for the following needle insertions. The user then followed the given path plans to complete 4 lumbar punctures at different inter-spinous gaps (2 at "Normal" lumbar and 2 at "Difficult" lumbar). The number of insertion trials until success were recorded for each location. Successful puncture insertions were defined as insertions where the needle tip reached the rubber tube embedded in the vertebral foramen. Successful and failed insertions were easily distinguished by the haptic feedback of inserting into the rubber tube, rather than hitting a rigid bone structure.

The same workflow was followed to perform another 4 sets of lumbar punctures with the second navigation interface. After performing the 8 lumbar puncture procedures in total, the user was asked to complete a questionnaire regarding the confidence and ergonomics of each planning and navigation interface. We performed a paired t-test to evaluate the statistical significance of the user questionnaire responses.

For this initial user study, we do not require the participants to have medical knowledge or experience with lumbar puncture, because our goal in this preliminary user study was (1) to evaluate the usability of each system for creating a needle plan, not the quality of the plan; (2) determine how well users could follow a predetermined needle plan using the visual guides in each system, which requires hand-eye coordination but no medical knowledge.

Study Results: A summary of the study results is shown in Fig. 9. Overall, our navigation systems showed a success rate of 89.1% on the first insertion trial. Users could reach the targets with an average of 1.14 and 1.12 needle insertion attempts when using the HoloLens and Tablet navigation systems, respectively. In our user survey, we found that users preferred the HoloLens 2 interface in the category of Insertion Confidence (P-value 0.03), whereas users showed no statistically significant preference in the other 3 domains.

IV. Discussion

Both the navigation accuracy experiments and user study results offer valuable insights regarding the confidence and

[2]https://github.com/liamjwang/patchus-lp-phantoms

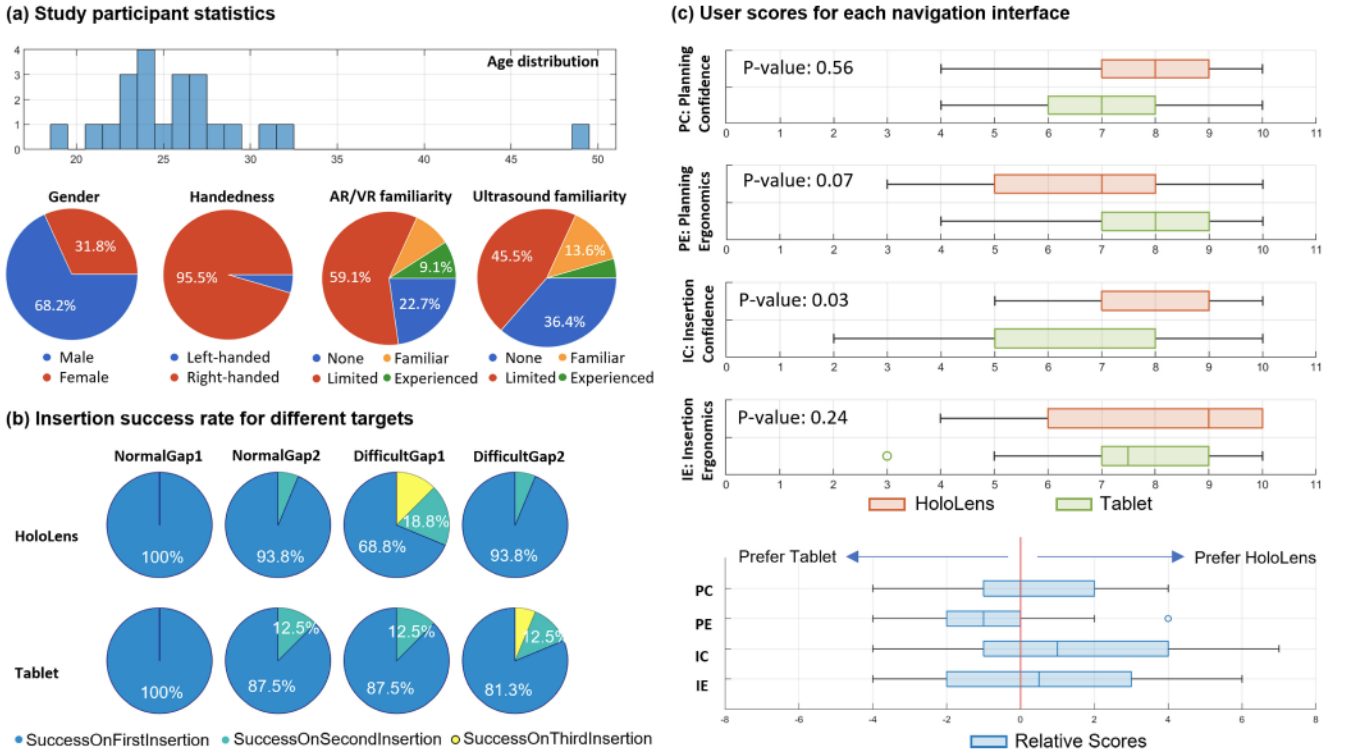

Fig. 9. User study statistical results. (a) 22 participants were recruited for the user study. (b) The number of attempts taken for successful insertion were recorded for each anatomical target and navigation interface. Note: the first 6 participants did not conduct the standard 8-insertion-trial procedure, so only the data from the last 16 participants are used for insertion success rate analysis. (c) Absolute and relative user scores for each interface, where relative scores are computed by subtracting the Tablet-score from the HoloLens-score from the same user in the same criterion. Paired t-test p-values are shown for each criterion.

ergonomics of the proposed systems, which we will discuss below.

A. *Navigation Accuracy Assessment Discussion*

Regarding the tracking accuracy assessment experiment, we anticipate that the accuracy variation across the workspace due to smoothly varying systematic tracking error would be minimal as the size of workspace is limited (about $20\,cm \times 20\,cm \times 20\,cm$ cube around the wearable ultrasound scanner) compared to the distance from the camera to the tracked object (2 meters for optical tracking, 0.5 meters for tablet camera tracking). By using the same marker on both the needle and wearable scanner, we intend to mitigate effects from systematic tracker error by only relying upon the relative positions between the wearable scanner and needle across the relatively small workspace.

In the end-to-end navigation accuracy assessment experiment, the fundamental assumption is that the needle tip is placed accurately at the cross-wire indentation with minimum needle bending, and the distance between the computed needle tip location and ultrasound-measured cross-wire point location should be 0 for a navigation system with no error. Therefore, the reported error metric in our system accuracy evaluation experiments in Section III-A encompass all navigation errors accumulated from scanner kinematics error, tracking inaccuracy, user annotation randomness, acoustic parameter settings and other calibration imperfections. Despite these challenges, our system can still achieve <3 mm accuracy for needle tip placement. One interesting byproduct of this experiment is the identification of the error attributed to the wearable ultrasound scanner itself. Because the wires and the scanner holder is a single piece of 3D printed phantom (Fig. 6(c)), and the placement of the scanner is a snug-fit sitting on the phantom, we know the theoretical location of the cross-wire points in the scanner's CAD model coordinates. Therefore, after comparing the annotations of the same sets of points identified in the ultrasound volume, we computed an error of 1.87 ± 0.67 mm for the four cross-wire point locations. This can be viewed as the theoretical imaging accuracy provided by the scanner itself. Although we do not have an extensive analysis to identify all the error sources, we expect the majority of the error comes from the following aspects – the calibration for the scanner kinematics, the imperfect speed-of-sound identification, the selection of cross-wire point locations from imaging, the tracking inaccuracies and the slight bending of the needle when placed on the cross-wire dent.

Other ultrasound needle guidance systems have reported accuracies of 1.03 ± 0.48 mm (mean $\pm$ SD) [23], 4.78 ± 2.28mm [16], and 0.9 ± 0.29 mm [34]. The results of our evaluation demonstrate that our system accuracy is comparable to those achieved by other guidance systems. Although some of these systems can be more accurate in point targeting, they lack several of the advantages of our system – they either do not provide volumetric imaging [23], [34] or require a bulky industrial robot with high motion accuracy [16].

The navigation accuracy requirement for lumbar puncture is highly patient-speci c. Given our dataset survey as presented in Figure 8, the size of the interspinous gap varies dramatically between 5 mm to 17 mm with an average around 10 mm, depending on the patient's age, gender, height, etc. For the normal-size phantom used in our user study, we picked on a subject with interspinous gap size of 11 mm, and another subject with a 7 mm gap for the dif cult-size phantom, which are both larger than the maximum navigation error reported as in Fig. 7. It was reported that for spine surgery, the error from the guidance system should be lower than 4 mm, and ideally below 2 mm [35], which is comparable to our overall system accuracy.

B. User Study Discussion

As shown in Fig. 9(a), majority of the participants have limited experience with ultrasound imaging or AR/VR application, and only one medical doctor is included. However, for this preliminary user study, our purpose is to test the basic components of our system to allow for further re nements before recruiting clinicians to participate in a larger scale clinical user study.

From Fig. 9(b), we can observe that both navigation interfaces can provide effective guidance for the LP procedures. It worth noting that we observed inferior performance of HoloLens-based guidance on target Dif cultGap1. We hypothesize that this may be an anatomy-speci c challenge (along with the imperfect surface estimation) where users may nd it harder to observe this anatomical gap and the visual guidance cues from the typical HoloLens perspective.

A slight user preference is seen for the different navigation interfaces. From Fig. 9(c), we observed that a statistically signi cant preference is shown towards the HoloLens-based system regarding the Insertion Con dence (IC) metric. This could be explained by the fact that the 3D spine surface model allowed the users to view the needle location within the entire inter-spinous gap from different viewing angles. For the other metrics, users showed no statistically signi cant preference between systems.

It is notable that there was a large amount of variation between users on the ergonomics and con dence metrics. We believe the large variation for the user scores comes from individual differences. From the qualitative feedback we received from the participants, individuals who struggled with the tablet interface often wanted to focus on both 2D and 3D guidance simultaneously and found it hard to control the needle to correctly align with the guidance cues in all views, whereas with the HoloLens they found the guidance to be more intuitive. Other individuals did not favor the HoloLens because they felt the need to move their hands and eyes signi cantly more during the process compared to the tablet interface in order to get high con dence for insertion.

For the user study, our goal was to compare the two navigation *systems* instead of making claims about which *device* is better. As such, we chose what we believe to be the most appropriate visualization for each device, rather than using identical visualizations. For instance, we elected not to display the bone surface on the tablet because it is dif cult to visualize a 3D mesh without requiring some form of user interaction to rotate the view, precluding hands-free use of the system. Additionally, the tablet does not provide the user with depth perception and is generally stationary during needle insertion, therefore the torus visual cue for showing tilt-error in the out-of-plane direction of the tablet was included. On the other hand, the HoloLens provides depth perception and allows the user to move their head to easily view the needle and navigation cues from different perspectives, therefore the 3D crosshair visual cues that show the expected needle placement within the spine are better suited to this visualization modality. While not a pure comparison of the visualization paradigms alone, this initial study demonstrates that both of these end-to-end systems perform well, but users demonstrate preferences in some domains for one system over the other. In subsequent user studies, we may attempt to subset out speci c components of each system that are preferred by clinical users.

Although not directly comparing with conventional methods of performing lumbar puncture, which may require a much more realistic palpable phantom and recruitment of LP experts, we compare against several other phantom studies for the general AR-guided needle insertion tasks that reported comparable metrics. A study by Park et al. [22] which conducted a CT-based AR phantom study found that their HoloLens-based system reduced the number of needle passes from 7.4 to 3.4 compared to conventional methods. Farshad-Amacker et al. [36] conducted a handheld 2D US-guided phantom study and found that their HoloLens-based system reduced needle passes from median[range] of 1[1-8] to 1[1-4]. While these studies use different techniques, our rst insertion success rate of 89.1% and average of 1.13 attempts in our preliminary user study demonstrates that the performance of our system compares favorably with other proposed systems.

C. Comparison Between the Two AR Navigation Systems

Our experiments and user study have shown that both of the presented AR systems demonstrate promising accuracy and usability. However, one of this work's main goals is to identify the best implementation for providing LP guidance to the clinician, so we summarize the key advantages (+) and disadvantages (–) of the two AR systems below.

Tablet-Based System:

+ Able to show raw ultrasound images that preserve important information so clinician with ultrasound experience will have higher con dence when making insertion plans.
+ It is a cheaper and more accessible solution.
+ It is easier to set up because it can be an integrated, self-contained computation and AR interface platform.
– Currently the tablet is only displaying 2D cross-section views of the acquired imaging data, which is less intuitive to make needle insertion plans.
– The tablet needs to be mounted between the patient and clinician, which can be less convenient to adjust dynamically for the best operation pose, considering also that the rear-facing camera must be able to track both the scanner and needle.

HoloLens-Based System:

+ According to our user study result, users have higher insertion confidence when guided by the HoloLens.
+ It is easy and intuitive to observe 3D anatomical information of the patient with our image processing pipeline.
+ The overall operation can be more comfortable because of a more natural and dynamic operating pose.
– Currently the needle/scanner tracking still depends on the external optical tracker, which is more expensive, complicated and may have line-of-sight issues.
– It is challenging to display raw ultrasound information on HoloLens, and the algorithm-processed patient model may be a less accurate representation.
– It can be difficult to operate with a power cord plugged in, so the battery life can be a potential limitation.
– It may be less comfortable to wear the head-mounted display during the procedure.

These feedbacks are crucial guidelines for us to adjust and develop the next generation of our system. For example, one way to integrate the strengths of both systems is for the clinician to use intuitive drag-and-drop actions to make plans in the HoloLens environment, while the plan path is visualized in real-time in the raw ultrasound images on the tablet screen for final confirmation.

V. Conclusion

Ultrasound guidance has been shown to significantly increase LP success rate and reduce the risk of complications. However, conventional ultrasound-guided lumbar puncture requires significant experience and coordination. This paper introduces a fully integrated lumbar puncture guidance system featuring a wearable ultrasound imaging device, bone reconstruction and segmentation algorithms, and augmented reality user interfaces, to provide multi-angle hands-free imaging in a more compact form factor. This setup also does not require preoperative imaging for complementary guidance information and can maintain the accurate image-anatomy relationship in the presence of patient motion throughout the procedure.

We have quantitatively validated the end-to-end needle targeting accuracy with each of the two navigation interfaces, and qualitatively evaluated the confidence and ergonomics of the proposed navigation systems via a phantom user study. The results show that promising accuracy and usability can be achieved to aid the user performing lumbar puncture.

In the future, we plan to improve the robustness of our navigation system to slight patient motion by using a biocompatible adhesive similar to the type used by the NeuroMD Corrective Therapy Device® to temporarily affix the wearable scanner to the patient's skin. We will validate the robustness to motion using a phantom mounted on a motion platform for simulating breathing and other slight movements. Additionally, we will test various clinically suggested scanner placement orientations. We also plan to recruit clinicians with LP experience to perform a user study on more realistic phantoms and demonstrate the improvement over conventional approach provided by our solution. Standarized image-guidance system scoring methods, such as [35], will also be employed in the user study to allow direct comparison with other approaches. In addition, we will continue to miniaturize the scanner into a "patch" form factor and develop autonomous ultrasound needle tracking during insertion to fully utilize the robotic capabilities of our scanner.

Acknowledgment

The authors acknowledge Razeyeh Bagherinasab for helping with the lumbar CT dataset segmentation and Dr. Ashraf Saad for suggestions on wearable ultrasound device integration.

References

[1] A. Vickers, J. P. Donnelly, J. X. Moore, S. R. Barnum, T. N. Schein, and H. E. Wang, "Epidemiology of lumbar punctures in hospitalized patients in the united states," *PLoS One*, vol. 13, no. 12, 2018, Art. no. e0208622.
[2] H. Kroll, R. Duszak Jr., E. Nsiah, D. R. Hughes, S. Sumer, and M. Wintermark, "Trends in lumbar puncture over 2 decades: A dramatic shift to radiology," *Amer. J. Roentgenol.*, vol. 204, no. 1, pp. 15–19, 2015.
[3] M. D. Seeberger, M. Kaufmann, S. Staender, M. Schneider, and D. Scheidegger, "Repeated dural punctures increase the incidence of postdural puncture headache," *Anesthesia Analgesia*, vol. 82, no. 2, pp. 302–305, 1996.
[4] E. Niemantsverdriet, H. Struyfs, F. Duits, C. E. Teunissen, and S. Engelborghs, "Techniques, contraindications, and complications of CSF collection procedures," *Cerebrospinal Fluid in Clinical Neurology*. Cham, Switzerland: Springer, 2015, pp. 35–57.
[5] C. Edwards, E. C. Leira, and P. Gonzalez-Alegre, "Residency training: A failed lumbar puncture is more about obesity than lack of ability," *Neurology*, vol. 84, no. 10, pp. e69–e72, 2015.
[6] J. Gorchynski, J. Oman, and T. Newton, "Interpretation of traumatic lumbar punctures in the setting of possible subarachnoid hemorrhage: Who can be safely discharged?" *California J. Emerg. Med.*, vol. 8, no. 1, pp. 3–7, 2007.
[7] S. J. Millington, M. S. Restrepo, and S. Koenig, "Better with ultrasound: Lumbar puncture," *Chest*, vol. 154, no. 5, pp. 1223–1229, 2018.
[8] N. J. Soni et al., "Ultrasound guidance for lumbar puncture," *Neurol. Clin. Pract.*, vol. 6, no. 4, pp. 358–368, 2016.
[9] N. J. Soni et al., "Recommendations on the use of ultrasound guidance for adult lumbar puncture: A position statement of the society of hospital medicine," *J. Hospital Med.*, vol. 14, no. 10, pp. 591–601, 2019.
[10] M. Gottlieb, D. Holladay, and G. D. Peksa, "Ultrasound-assisted lumbar punctures: A systematic review and meta-analysis," *Acad. Emerg. Med.*, vol. 26, no. 1, pp. 85–96, 2019.
[11] T. De Silva et al., "Real-time, image-based slice-to-volume registration for ultrasound-guided spinal intervention," *Phys. Med. Biol.*, vol. 63, no. 21, 2018, Art. no. 215016.
[12] H.-E. Gueziri, S. Drouin, C. X. Yan, and D. L. Collins, "Toward real-time rigid registration of intra-operative ultrasound with preoperative CT images for lumbar spinal fusion surgery," *Int. J. Comput. Assist. Radiol. Surg.*, vol. 14, no. 11, pp. 1933–1943, 2019.
[13] L. Ma, Z. Zhao, F. Chen, B. Zhang, L. Fu, and H. Liao, "Augmented reality surgical navigation with ultrasound-assisted registration for pedicle screw placement: A pilot study," *Int. J. Comput. Assist. Radiol. Surg.*, vol. 12, pp. 2205–2215, Dec. 2017.
[14] I. Hacihaliloglu, A. Rasoulian, R. N. Rohling, and P. Abolmaesumi, "Local phase tensor features for 3-D ultrasound to statistical shape+pose spine model registration," *IEEE Trans. Med. Imag.*, vol. 33, no. 11, pp. 2167–2179, Nov. 2014.
[15] M. H. Mozaffari and W.-S. Lee, "Freehand 3-D ultrasound imaging: A systematic review," *Ultrasound Med. Biol.*, vol. 43, no. 10, pp. 2099–2124, 2017.
[16] J. Esteban et al., "Robotic ultrasound-guided facet joint insertion," *Int. J. Comput. Assist. Radiol. Surg.*, vol. 13, pp. 895–904, Jun. 2018.
[17] J. Moore et al., "Image guidance for spinal facet injections using tracked ultrasound," in *Proc. Med. Image Comput. Comput.-Assist. Intervent. (MICCAI)*, 2009, pp. 516–523.
[18] O. Zettinig et al., "Toward real-time 3D ultrasound registration-based visual servoing for interventional navigation," in *Proc. IEEE Int. Conf. Robot. Autom. (ICRA)*, 2016, pp. 945–950.

[19] H. K. Zhang et al., "Toward dynamic lumbar puncture guidance using needle-based single-element ultrasound imaging," *J. Med. Imag.*, vol. 5, no. 2, 2018, Art. no. 21224.

[20] K. Xu, Y. Kim, E. M. Boctor, and H. K. Zhang, "Enabling low-cost point-of-care ultrasound imaging system using single element transducer and delta con guration actuator," in *Proc. Med. Imag. Guided Proced. Robot. Intervent. Model.*, vol. 10951, 2019, pp. 224–230.

[21] J. Tanwani et al., "Development of a head-mounted holographic needle guidance system for enhanced ultrasound-guided neuraxial anesthesia: System development and observational evaluation," *JMIR Formative Res.*, vol. 6, no. 6, 2022, Art. no. e36931.

[22] B. J. Park, S. J. Hunt, G. J. Nadolski, and T. P. Gade, "Augmented reality improves procedural ef ciency and reduces radiation dose for CT-guided lesion targeting: A phantom study using HoloLens 2," *Sci. Rep.*, vol. 10, no. 1, pp. 1–8, 2020.

[23] T. Ungi et al., "Spinal needle navigation by tracked ultrasound snapshots," *IEEE Trans. Biomed. Eng.*, vol. 59, no. 10, pp. 2766–2772, Oct. 2012.

[24] K. Xu, B. Jiang, A. Moghekar, P. Kazanzides, and E. Boctor, "AutoInFocus, a new paradigm for ultrasound-guided spine intervention: A multi-platform validation study," *Int. J. Comput. Assist. Radiol. Surg.*, vol. 17, no. 5, pp. 911–920, 2022.

[25] B. Jiang, K. Xu, A. Moghekar, P. Kazanzides, and E. Boctor. "Feature-aggregated spatiotemporal spine surface estimation for wearable patch ultrasound volumetric imaging." 2022. [Online]. Available: https://arxiv.org/abs/2211.05962.

[26] E. Olson, "AprilTag: A robust and exible visual ducial system," in *Proc. IEEE Int. Conf. Robot. Autom.*, 2011, pp. 3400–3407.

[27] O. V. Solberg, F. Lindseth, H. Torp, R. E. Blake, and T. A. N. Hernes, "Freehand 3D ultrasound reconstruction algorithms—A review," *Ultrasound Med. Biol.*, vol. 33, no. 7, pp. 991–1009, 2007.

[28] N. Otsu, "A threshold selection method from gray-level histograms," *IEEE Trans. Syst., Man, Cybern.*, vol. 9, no. 1, pp. 62–66, Jan. 1979.

[29] W. Schroeder, R. Maynard, and B. Geveci, "Flying edges: A high-performance scalable isocontouring algorithm," in *Proc. IEEE 5th Symp. Large Data Anal. Visualizat. (LDAV)*, 2015, pp. 33–40.

[30] A. Fedorov et al., "3D slicer as an image computing platform for the quantitative imaging network," *Mag. Reson. Imag.*, vol. 30, no. 9, pp. 1323–1341, 2012.

[31] J. Saltz et al. "Stony brook university COVID-19 positive cases [data set], cancer imaging archive." 2021. [Online]. Available: https://doi.org/10.7937/TCIA.BBAG-2923

[32] K. Clark et al., "The cancer imaging archive (TCIA): Maintaining and operating a public information repository," *J. Digit. Imag.*, vol. 26, no. 6, pp. 1045–1057, 2013.

[33] S.-L. Chao, K.-C. Chen, L.-W. Lin, T.-L. Wang, and C.-F. Chong, "Ultrasound phantoms made of gelatin covered with hydrocolloid skin dressing," *J. Emerg. Med.*, vol. 45, no. 2, pp. 240–243, 2013.

[34] S. Chen, F. Wang, Y. Lin, Q. Shi, and Y. Wang, "Ultrasound-guided needle insertion robotic system for percutaneous puncture," *Int. J. Comput. Assist. Radiol. Surg.*, vol. 16, pp. 475–484, Mar. 2021.

[35] K. Móga, A. Ferencz, and T. Haidegger, "What is next in computer-assisted spine surgery? advances in image-guided robotics and extended reality," *Robotics*, vol. 12, no. 1, p. 1, 2022.

[36] N. A. Farshad-Amacker et al., "Ultrasound-guided interventions with augmented reality in situ visualisation: A proof-of-mechanism phantom study," *Eur. Radiol. Exp.*, vol. 4, no. 1, pp. 1–7, 2020.